Shielding effect of radiation dose reduction fiber during the use of C-arm fluoroscopy: a phantom study

Hyemi Cha[1], Kisung Lee[1], Moon Seok Park[2], Kyoung Min Lee[2], Kyeyoung Cho[1] and Ki Hyuk Sung[2],*

[1]Department of Bio-convergence Engineering, Korea University, Seoul, Korea
[2]Department of Orthopaedic Surgery, Seoul National University Bundang Hospital, Gyeonggi, Korea
*Corresponding author. Department of Orthopaedic Surgery, Seoul National University Bundang Hospital, 82 Gumi-ro 173 Beon-gil, Bundang-Gu, Sungnam, Gyeonggi 13620, Korea. Tel: 82-31-787-7207; Fax: 82-31-787-4056; Email: skh1219@naver.com
(Received 25 February 2020; revised 1 June 2020; editorial decision 10 July 2020)

ABSTRACT

This study evaluated the shielding effect of a newly developed dose-reduction fiber (DRF) made from barium sulfate, in terms of radiation doses delivered to patients' radiosensitive organs and operator during C-arm fluoroscopy and its impact on the quality of images. A C-arm fluoroscopy unit was placed beside a whole-body phantom. Radiophotoluminescent glass dosimeters were attached to the back and front of the whole-body phantom at 20 cm intervals. Radiation doses were measured without DRF and with it applied to the back (position 1), front (position 2) or both sides (position 3) of the phantom. To investigate the impact of DRF on the quality of fluoroscopic images, step-wedge and modulation transfer function phantoms were used. The absorbed radiation doses to the back of the phantom significantly decreased by 25.3–88.8% after applying DRF to positions 1 and 3. The absorbed radiation doses to the front of the phantom significantly decreased by 55.3–93.6% after applying DRF to positions 2 and 3. The contrast resolution values for each adjacent step area fell in the range 0.0119–0.0209, 0.0128–0.0271, 0.0135–0.0339 and 0.0152–0.0339 without and with DRF applied to positions 1, 2 and 3, respectively. The investigated DRF effectively reduces absorbed radiation doses to patients and operators without decreasing the quality of C-arm fluoroscopic images. Therefore, routine clinical use of the DRF is recommended during the use of C-arm fluoroscopy.

Keywords: dose reduction fiber; barium sulfate; radiation dose; C-arm fluoroscopy

INTRODUCTION

Since X-rays were discovered in 1895 by Roentgen, radiographic imaging modalities, including conventional radiography, computed tomography (CT) and fluoroscopy, are widely used in the medical field as diagnostic and treatment tools. Of these, C-arm fluoroscopy has been widely used in operating rooms during various procedures, such as orthopedic surgery, spine procedures and vascular interventions, because it can provide real-time images of anatomical structures [1–3].

With the use of C-arm fluoroscopy increasing, there have been concerns about the amount of radiation exposure to operators [4–6]. Especially, radiation exposure should be minimized for radiosensitive organs, including the gonads, lens of the eyes, thyroid, breast and thymus [7, 8]. To reduce radiation exposure for operators, radio-protective garments, including lead apron, thyroid shields, radiation reducing gloves and goggles, are mostly used during C-arm fluoroscopy. Similar to operators, patients on the operating table are also vulnerable to direct and scattered radiation. A number of studies investigated the radiation doses received by the operator and identified the factors that could reduce radiation exposure [4, 8–13]. However, patient exposure during C-arm fluoroscopy has been studied less extensively compared with operator exposure.

Recently, a dose reduction fiber (DRF) shielding cloth (DRF®, RADTECH Korea, Gyeongju, Korea) was developed to reduce the radiation dose to patients (Fig. 1). DRF was made from barium sulfate ($BaSO_4$) and its thickness was 2 mm, which corresponded to the lead equivalent of 0.1 mm Pb. However, no study has investigated the protective effect of the newly developed DRF shielding cloth. Therefore,
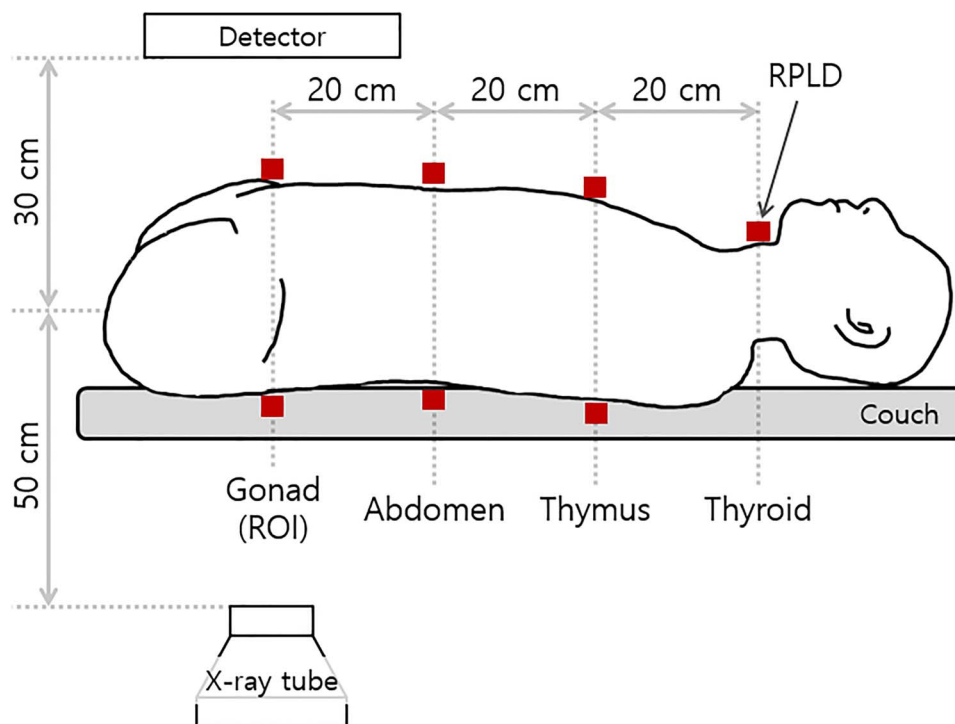
Fig. 1. Experimental setup for measurement of absorbed radiation doses.

we performed this study to evaluate the shielding effect of DRF in terms of radiation doses delivered to patients' radiosensitive organs and the operator during the use of C-arm fluoroscopy. In addition, we investigated the impact of DRF on the quality of C-arm fluoroscopic images.

MATERIALS AND METHODS

This study was exempted from the approval of our institutional review board because it did not involve human subjects.

A whole-body phantom (PBU-60; Kyoto Kagaku CO., LTD., Kyoto, Japan) was placed on the operating table to simulate a patient. The whole-body phantom was composed of a cadaver bone surrounded by soft-tissue-equivalent acrylic material that had approximately the same density as human soft tissue. A C-arm fluoroscopy unit (OEC 9800; GE Healthcare, Milwaukee, WI, USA) was placed beside the whole-body phantom at a 90° angle in the standard posteroanterior (PA) position (with the X-ray tube placed downward and the detector placed upward). The distance between the whole-body phantom and the C-arm detector was 30 cm (Fig. 1). The C-arm fluoroscopy unit was focused on the pelvis at the automatic energy setting of 85 kvP and 3.5 mAs.

Radiophotoluminescent glass dosimeters (RPLD, GD-352 M; AGC Techno Glass, Tokyo, Japan) were attached to the back and front of the whole-body phantom at the position of the thyroid, thymus, abdomen and gonads with an interval of 20 cm (Fig. 1).

First, radiation doses to the back of the phantom at the position of the gonads, abdomen and thymus, and to the front of the phantom at the position of gonads, abdomen, thymus and thyroid were measured

by RPLD without DRF as control. Thereafter, DRF was applied to the back (position 1), front (position 2) or both sides (position 3) of the whole-body phantom and radiation doses were measured again. When DRF was applied to the back of the whole-body phantom, RPLD were located between the DRF and the whole-body phantom. When DRF was applied to the front of the phantom, RPLD were located above the DRF (Fig. 2). The whole-body phantom was exposed to the radiation source for 10 min, and the absorbed radiation doses were recorded by the RPLD. For each scenario, the experiment was repeated 10 times, and the average absorbed radiation dose per minute was calculated.

To compare the impact of DRF on the quality of images, a step wedge phantom (CIRS model 018) and modulation transfer function (MTF) phantom (Type 52) were used. Each phantom was located on the operating table and the phantom images from the C-arm fluoroscopy unit with the automatic energy setting of 60 kvP and 1.4 mAs were obtained.

The step-wedge phantom images were used to calculate the contrast resolution (CR) that describes the difference between two target regions of interest (ROIs) [14]. The step-wedge phantom contained 11 steps and every step was included in the field of view. The CR of each step was calculated according to the following equation:

$$CR = \frac{S_A - S_B}{S_A + S_B}$$

where S_A and S_B are the signal intensity defined as the sum of the pixel values in the ROI of adjacent steps. The ROI was an area of 10×100 pixels that was boxed in each step area at the same position in the step phantom image. The step phantom images with and without use of
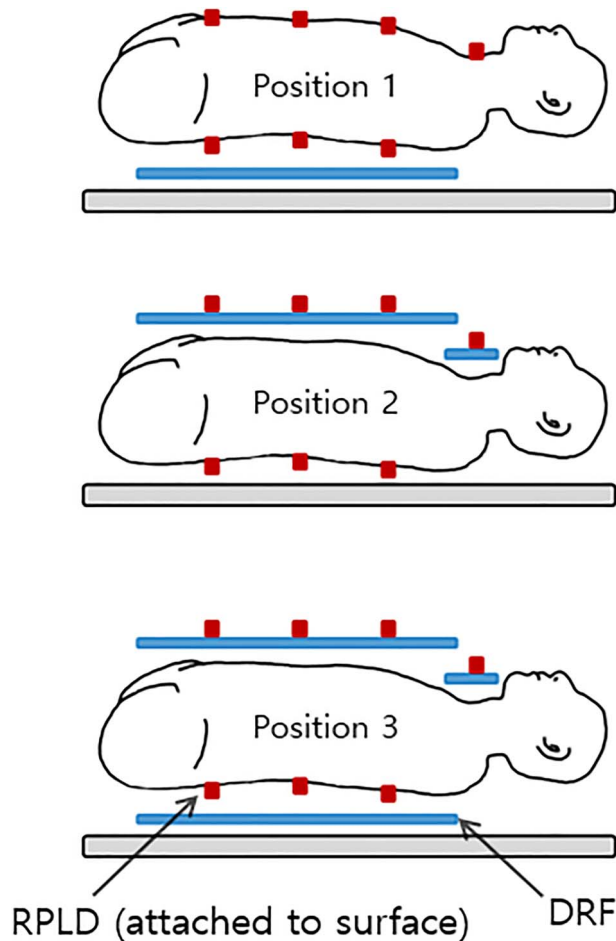
Fig. 2. Location of radiophotoluminescent glass dosimeters (RPLD) and dose reduction fiber (DRF) at positions 1, 2 and and 3.

DRF were obtained under the same conditions as in the whole-body phantom experiments.

The MTF phantom images were used to analyze the spatial resolution using the MTF. The MTF was defined as the contrast at a given spatial frequency compared with the contrast at a low frequency according to the following equation:

$$\text{MTF} = \frac{C(f)}{C(0)} \times 100 \ (\%)$$

where $C(0)$ was the lowest frequency contrast, assumed to be the spatial frequency of 0 LP/mm, while the contrast $C(f)$ at spatial frequency f was calculated as shown below:

$$C(f) = \frac{V_{max} - V_{min}}{V_{max} + V_{min}}$$

where V_{max} and V_{min} were the average values of the peak and the valley in the pattern image of each spatial frequency.

Statistical methods

The Kolmogorov–Smirnov test was used to identify the normality of continuous variables. The Kruskal–Wallis test was used to analyze the differences in absorbed radiation doses according to the use of DRF. Multiple comparison tests were performed using Bonferroni correction. All statistical analyses were performed using SPSS software for Windows (version25.0; SPSS, Inc., Chicago, IL, USA). All statistics were two-tailed, and P-values < 0.05 were considered statistically significant.

RESULTS

For the back of the whole-body phantom without DRF, the absorbed radiation doses at the location of the thymus (122.3 μSv/min) and abdomen (378.6 μSv/min) were 0.7 and 2.3% of those absorbed at the location of the gonads (16369.7 μSv/min). Radiation doses at the location of the thymus, abdomen and gonads decreased significantly after applying DRF to the back of the phantom ($P < 0.001$) and to the both sides of the phantom ($P < 0.001$). Moreover, the absorbed radiation doses to the back of the phantom decreased by 25.3–42.9% as a result of DRF use at the back of the phantom and by 34.2–88.8% as a result of DRF use at both sides of the phantom (Fig. 3).

For the front of the whole-body phantom without DRF, the absorbed radiation doses at the location of the thyroid (70.3 μSv/min), thymus (69.9 μSv/min) and abdomen (111.5 μSv/min) were 14.6, 14.5 and 23.2% of those absorbed at the location of the gonads (480.6 μSv/min). When DRF was applied to the front of the phantom and to both sides of the phantom, the absorbed radiation doses to the front of the phantom significantly decreased by 55.3–93.6% (all $P < 0.001$). When DRF was applied to the back of the phantom, the absorbed radiation doses significantly decreased at the location of the gonads by 35.3% and at the location of the abdomen by 4.7%, but increased at the location of the thymus by 20.1% and at the location of the thyroid by 5.9% (all $P < 0.001$) (Fig. 4).

The CR values for each adjacent step area fell in the range 0.0119–0.0209, 0.0128–0.0271, 0.0135–0.0339 and 0.0152–0.0339 for the experiment without DRF and with DRF applied to positions 1, 2 and 3, respectively (Fig. 5). The average values of the CR with DRF were increased compared with the average value without DRF. The rates of increase according to the position of the DRF were 18.8, 17.9 and 43.4%, respectively, for positions 1–3.

Figure 6 shows the MTF curves without DRF and with DRF located at positions 1–3, and the trend of the MTF curve shape shows little difference for all cases. Comparing MTF values of each LP/mm, the performance was reduced by 8.4, 2.3 and 19.1% respectively, according to the position of the DRF. The MTF performance in the low frequency area was not significantly different, but in the high frequency area between 1.4 and 2.0 LP/mm, the MTF performance was decreased when DRF was used, especially at position 3.

DISCUSSION

Previous studies demonstrated the effect of barium sulfate composite thyroid collars and apron on radiation protection for operators during the use of fluoroscopy and X-ray [15, 16]. However, there has been
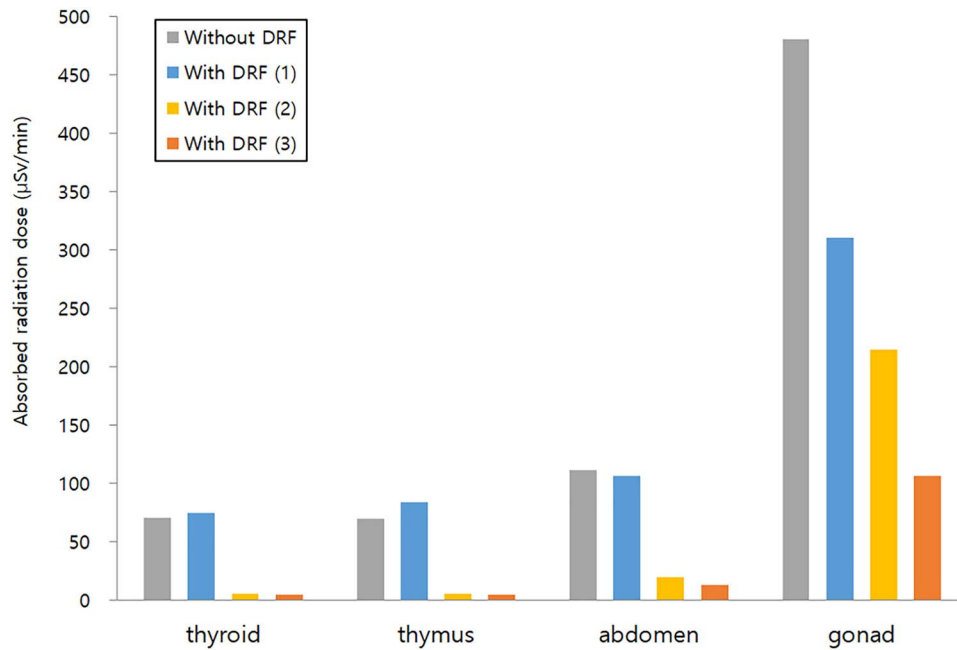
Fig. 3. Comparison of absorbed radiation doses to the front of the whole-body phantom at the location of the thyroid, thymus, abdomen and gonads without DRF and with it applied to the back (position 1), and both sides (position 3) of the phantom.
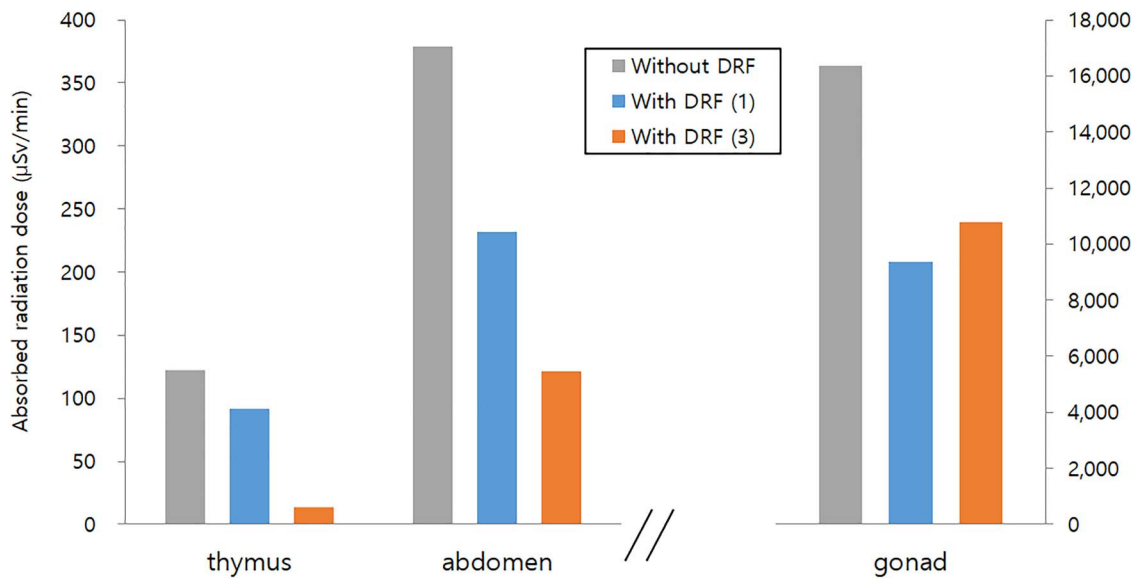

Fig. 4. Comparison of absorbed radiation doses to the back of the whole-body phantom at the location of the thymus, abdomen and gonads without DRF and with it applied to the back (position 1), and both sides (position 3) of the phantom.

no study investigating the effect of patient organ shield during C-arm fluoroscopic examination. The current study demonstrated that the newly developed DRF shielding cloth could reduce the absorbed radiation doses to patients and operators. In addition, the quality of C-arm fluoroscopic images was not affected by DRF application.

There are limitations to this study. First, the radiation doses of the front of the whole-body phantom did not accurately indicate the radiation dose to the operator because of the distance between the patient and the operator, and scattering. Further study using the operator phantom is required to measure the scattered radiation doses to
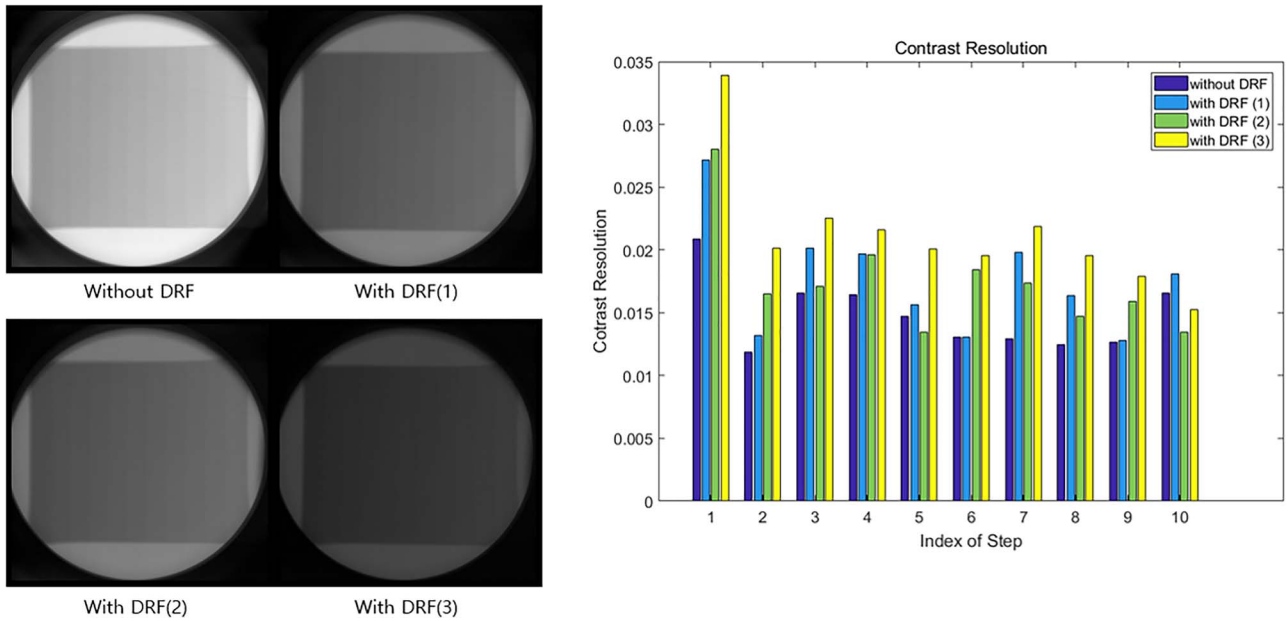
Fig. 5. Images and contrast resolution of the step-wedge phantom from the C-arm fluoroscopy obtained without DRF and with it applied to the back (position 1), front (position 2) and both sides (position 3) of the phantom.
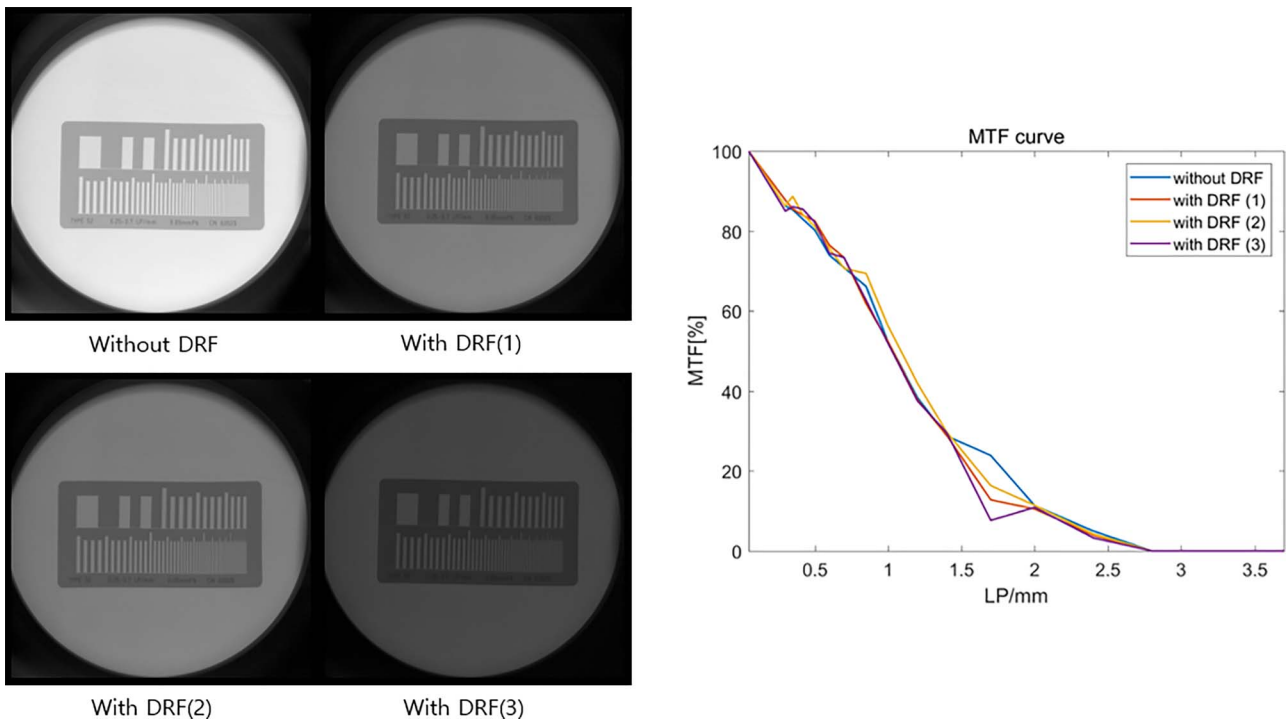

Fig. 6. Images and modulation transfer function (MTF) curves of the MTF phantom from the C-arm fluoroscopy obtained without DRF and with it applied to the back (position 1), front (position 2) and both sides (position 3) of the phantom.

the operator more accurately. Second, this study may overestimate the absorbed radiation doses to patients' radiosensitive organs because the RPLDs were attached to the outer surface of the whole-body phantom.

Third, we did not evaluate the effect of the operating table on the radiation dose. The materials and thickness of the operating table may be important factors that could affect the radiation dose. However,

we used the operating table that was used in actual clinical practice; thus, our study's results are clinically meaningful. Fourth, the energy setting of C-arm fluoroscopy could affect the image quality. Further study regarding image quality according to the energy setting of C-arm fluoroscopy is required.

When RPLD were attached to the back of the phantom, the absorbed radiation dose to ROI of C-arm fluoroscopy was 43 and 134 times higher than that in regions at 20 and 40 cm distance from ROI, respectively. When RPLD was applied on the front of the phantom, the absorbed radiation dose to ROI of C-arm fluoroscopy was 4, 7 and 7 times higher than that in regions at 20, 40 and 60 cm distance from the ROI, respectively. Therefore, we think that patients should be protected using this dose-reduction shield, especially at the ROI of C-arm fluoroscopy.

In terms of absorbed radiation doses to the operator from C-arm fluoroscopy, our experiment found that the application of DRF to both front and back sides of the patient can reduce the radiation doses most effectively. In terms of absorbed radiation doses to the patient, the DRF attached to both sides of patients also decreased the radiation dose most effectively, except for the ROI of C-arm fluoroscopy. Therefore, the application of DRF to both front and back sides of patients can be recommended to reduce the absorbed radiation doses to both patients and operators during the use of C-arm fluoroscopy.

As the number of CT examinations performed continues to increase, radiation doses for patients have also increased [17, 18]. The radiation doses delivered by CT are 100–500 times higher than those of conventional radiography and are associated with increased cancer risk [19]. Furthermore, children are more sensitive to radiation-induced carcinogenesis compared with adults [19, 20]. Therefore, radiation exposure should be minimized for patients' radiosensitive organs, such as the lenses of the eyes, thyroid, breast and gonads during CT scanning. Several studies evaluated the effect of the bismuth shield on radiation-dose reduction for radiosensitive organs in patients who underwent CT [21–23]. They reported radiation dose reductions of 1.2–60%, depending on the organs and CT protocol. A meta-analysis demonstrated that the bismuth shield was effective in decreasing the patients' surface radiation dose by decreasing the low-energy photons delivered at its surface during CT scanning [24]. In our experiments, 25.3–88.8% radiation-dose reduction was observed in patients during C-arm fluoroscopy. We think that our newly developed DRF from barium sulfate can also be used during CT scanning. To confirm the shielding effect of the DRF during CT scanning, further experiments using DRF are required.

For the dose-reduction shield to be commercially available, the quality of radiographic images should be maintained. Bismuth shields are easy to use and have been known to reduce radiation doses without creating artifacts, while general lead shields can cause streak and beam-hardening artifacts. Several studies demonstrated the shielding effect of bismuth or barium sulfate shields without any substantial deterioration of image quality [21, 25]. In our experiments, the quality of the C-arm fluoroscopic images did not decrease after applying the DRF to the front or back of the phantom. However, the image quality decreased when the DRF was applied to both sides of the phantom. Therefore, we recommend the use of DRF to the back side of patients in ROI, and both front and back sides of the patients in other regions, to maximize the radiation dose-reduction effect in both the patient and the operator, and to preserve image quality during C-arm fluoroscopy.

In conclusion, this study showed that the newly developed DRF shielding cloth made from barium sulfate is effective in reducing the absorbed radiation doses to both patients and operators. In addition, the shielding effect of DRF can be obtained without decreasing the quality of C-arm fluoroscopic images. Therefore, routine clinical use of this DRF can be recommended during C-arm fluoroscopy.

CONFLICT OF INTEREST

None declared.

FUNDING

REFERENCES

1. Gavit L, Carlier S, Hayase M et al. The evolving role of coronary angiography and fluoroscopy in cardiac diagnosis and intervention. *EuroIntervention* 2007;2:526–32.
2. Huang AJ. Fluoroscopically guided lumbar facet joint injection using an interlaminar approach and loss of resistance technique. *Skeletal Radiol* 2016;45:671–6.
3. Dawe EJ, Fawzy E, Kaczynski J et al. A comparative study of radiation dose and screening time between mini C-arm and standard fluoroscopy in elective foot and ankle surgery. *Foot Ankle Surg* 2011;17:33–6.
4. Shoaib A, Rethnam U, Bansal R et al. A comparison of radiation exposure with the conventional versus mini C arm in orthopedic extremity surgery. *Foot Ankle Int* 2008;29:58–61.
5. Mesbahi A, Rouhani A. A study on the radiation dose of the orthopaedic surgeon and staff from a mini C-arm fluoroscopy unit. *Radiat Prot Dosimetry* 2008;132:98–101.
6. Tuohy CJ, Weikert DR, Watson JT et al. Hand and body radiation exposure with the use of mini C-arm fluoroscopy. *J Hand Surg Am* 2011;36:632–8.
7. Biswas D, Bible JE, Bohan M et al. Radiation exposure from musculoskeletal computerized tomographic scans. *J Bone Joint Surg Am* 2009;91:1882–9.
8. Lee K, Lee KM, Park MS et al. Measurements of surgeons' exposure to ionizing radiation dose during intraoperative use of C-arm fluoroscopy. *Spine (Phila Pa 1976)* 2012;37:1240–4.
9. Sung KH, Jung YJ, Kwon SS et al. Performances of a protector against scattered radiation during intraoperative use of a C-arm fluoroscope. *J Radiol Prot* 2016;36:629–40.
10. Sung KH, Min E, Chung CY et al. Measurements of surgeons' exposure to ionizing radiation dose: Comparison of conventional and mini C-arm fluoroscopy. *J Hand Surg Eur Vol* 2016;41:340–5.

11. Sung KH, Jung YJ, Cha H et al. Effect of metallic tools on scattered radiation dose during the use of C-arm fluoroscopy in orthopaedic surgery. *J Radiat Res* 2019;60:1–6.

12. Lee SY, Min E, Bae J et al. Types and arrangement of thyroid shields to reduce exposure of surgeons to ionizing radiation during intraoperative use of C-arm fluoroscopy. *Spine (Phila Pa 1976)* 2013;38:2108–12.

13. Rehani MM, Ciraj-Bjelac O, Vano E et al. ICRP publication 117. Radiological protection in fluoroscopically guided procedures performed outside the imaging department. *Ann ICRP* 2010;40:1–102.

14. Prince JL, Links JM. *Medical Imaging Signals and Systems*. New Jersey: Pearson Prentice Hall, 2006.

15. Kim SC, Choi JR, Jeon BK. Physical analysis of the shielding capacity for a lightweight apron designed for shielding low intensity scattering X-rays. *Sci Rep* 2016;6:27721.

16. Uthoff H, Benenati MJ, Katzen BT et al. Lightweight bilayer barium sulfate-bismuth oxide composite thyroid collars for superior radiation protection in fluoroscopy-guided interventions: A prospective randomized controlled trial. *Radiology* 2014;270:601–6.

17. Fazel R, Krumholz HM, Wang Y et al. Exposure to low-dose ionizing radiation from medical imaging procedures. *N Engl J Med* 2009;361:849–57.

18. Brenner DJ, Hall EJ. Computed tomography–an increasing source of radiation exposure. *N Engl J Med* 2007;357:2277–84.

19. Miglioretti DL, Johnson E, Williams A et al. The use of computed tomography in pediatrics and the associated radiation exposure and estimated cancer risk. *JAMA Pediatr* 2013;167:700–7.

20. Hartin CW Jr, Jordan JM, Gemme S et al. Computed tomography scanning in pediatric trauma: Opportunities for performance improvement and radiation safety. *J Surg Res* 2013;180:226–31.

21. Catuzzo P, Aimonetto S, Fanelli G et al. Dose reduction in multislice CT by means of bismuth shields: Results of in vivo measurements and computed evaluation. *Radiol Med* 2010;115:152–69.

22. Chang KH, Lee W, Choo DM et al. Dose reduction in CT using bismuth shielding: Measurements and Monte Carlo simulations. *Radiat Prot Dosimetry* 2010;138:382–8.

23. Hohl C, Wildberger JE, Suss C et al. Radiation dose reduction to breast and thyroid during MDCT: Effectiveness of an in-plane bismuth shield. *Acta Radiol* 2006;47:562–7.

24. Mehnati P, Malekzadeh R, Sooteh MY. Use of bismuth shield for protection of superficial radiosensitive organs in patients undergoing computed tomography: A literature review and meta-analysis. *Radiol Phys Technol* 2019;12:6–25.

25. Huggett J, Mukonoweshuro W, Loader R. A phantom-based evaluation of three commercially available patient organ shields for computed tomography X-ray examinations in diagnostic radiology. *Radiat Prot Dosimetry* 2013;155:161–8.